Nano Research 2018, 11(1): 163–173
https://doi.org/10.1007/s12274-017-1615-2
Research Article
ISSN 1998-0124
CN 11-5974/O4

Metal-organic framework-derived, Zn-doped porous carbon polyhedra with enhanced activity as bifunctional catalysts for rechargeable zinc-air batteries

Xuan Wu[§], Ge Meng[§], Wenxian Liu, Tian Li, Qiu Yang, Xiaoming Sun, and Junfeng Liu (✉)

State Key Laboratory of Chemical Resource Engineering, Beijing University of Chemical Technology, Beijing 100029, China
[§] Xuan Wu and Ge Meng contributed equally to this work.

Received: 6 January 2017
Revised: 30 March 2017
Accepted: 7 April 2017

KEYWORDS
Zn-doped Co-MOF, porous carbon polyhedra, oxygen reduction reaction, oxygen evolution reaction, zinc-air batteries

ABSTRACT

Zinc-air batteries have recently attracted considerable interest owing to the larger storage capacity and lower cost compared to their lithium-ion counterparts. Electrode catalysts for the oxygen reduction reaction (ORR) and oxygen evolution reaction (OER) play a critical role in the operation of rechargeable zinc-air batteries. Herein, we report a simple and scalable strategy to fabricate porous carbon polyhedra using Zn-doped Co-based zeolitic imidazolate frameworks (ZnCo-ZIFs) as precursors. Strikingly, Zn doping leads to smaller Co nanoparticles and higher nitrogen content, which in turn enhances the ORR and OER activities of the obtained porous carbon polyhedra. The synergistic effect of the N-doped carbon and cobalt nanoparticles in the composite, the improved conductivity resulting from the high graphitization of carbon, and the large surface area of the porous polyhedral structure resulted in porous carbon polyhedra with excellent ORR and OER electrocatalytic activity in alkaline media. More importantly, air cathodes based on the optimal porous carbon polyhedra further exhibited superior performance to Pt/C catalysts in primary and rechargeable zinc-air batteries.

1 Introduction

Energy storage represents one of the great challenges of the twenty-first century. To meet the specific requirements of electric and hybrid vehicles, significant research efforts are focusing on the development of low-cost and environmentally friendly systems for energy conversion and storage [1]. Recently, rechargeable metal-air (such as zinc- and lithium-air) batteries have attracted significant interest owing to their high theoretical energy capacities [2–4]. Zinc-air batteries, in particular, represent a very promising technology with several potential benefits, including low cost, high safety, and environmentally friendly operation [5]. Rechargeable zinc-air batteries require active and durable cathode electrocatalysts capable

Address correspondence to ljf@mail.buct.edu.cn

of efficiently catalyzing both the oxygen reduction reaction (ORR) and oxygen evolution reaction (OER) [6, 7]. Although Pt-, Ru-, or Ir-based materials are the most efficient ORR or OER catalysts, their high cost and limited availability severely hinder their wide applicability. As an alternative to these materials, N-doped carbon materials incorporating transition metals/oxides have been actively investigated as bifunctional ORR and OER catalysts because of their high activity, high stability, and low cost [8, 9]. For example, Dai and coworkers grew Co_3O_4 nanocrystals on N-doped graphene and found that the hybrid material exhibited excellent performance in the ORR and OER processes, owing to the synergistic effect of the two components [10]. Chen and coworkers reported a synergistic catalyst consisting of Co nanoparticles embedded in N-doped carbon, which exhibited high catalytic activity toward both ORR and OER [11]. Although several studies have reported the synthesis of N-doped carbon materials incorporating metal/oxide as bifunctional ORR and OER catalysts, there is still considerable interest in the development of methods for obtaining catalysts with high surface area and uniform distribution of active sites.

Metal-organic frameworks (MOFs) are among the most attractive porous materials and consist of metal ions coordinated to organic molecules to form diverse architectures [12–18]. MOFs have proven effective as precursors or sacrificial templates to prepare derivatives with the corresponding inherited morphology, such as metal or metal oxide semiconductors [19–22], N-doped nanoporous carbon [23–25], and their composite nanostructures [26–29]. The well-organized framework can be converted to porous carbon with high surface area and uniform N- or S-doping via thermal activation, taking advantage of the partially preserved porosity of MOFs containing N- or S-based ligands; this procedure leads to porous carbon with highly improved electrocatalytic performance [30]. At the same time, the metal cations will be converted to metal or metal oxide with uniformly distribution in the porous carbon, where they can behave as highly active sites for electrochemical reactions [31]. For example, Jiang and coworkers synthesized porous carbons with high surface area, high graphitization degree, and uniform distributions of CoN_x and N dopants using bimetallic zeolitic imidazolate frameworks (based on ZIF-8 and ZIF-67) as templates/precursors. Upon additional P doping, the ORR activity of multicomponent doped carbon can be further boosted, exceeding that of Pt/C and most non-precious metal catalysts [32]. Some bifunctional ORR and OER electrocatalysts have already been prepared from MOF precursors. For example, Lou and coworkers used the ZIF-67 template to synthesize N-doped carbon nanotubes with hollow frameworks, which exhibited excellent ORR and OER electrocatalytic activity [33]. Nevertheless, very few reports on the application of these materials as bifunctional electrocatalysts in efficient metal-air battery devices have been published.

Therefore, in this manuscript we report an efficient strategy (Fig. 1) to fabricate new bifunctional electrocatalysts composed of porous carbon polyhedra, using Zn-doped Co-ZIFs based on ZIF-8 and ZIF-67 structures and containing different Zn/Co ratios as templates/precursors. The corresponding catalysts are labeled ZnCoNC-*x*, where *x* denotes the Zn/Co molar ratio. Doping with Zn species not only reduces the Co nanoparticle size but also increases the nitrogen content of the products; this endows the as-prepared

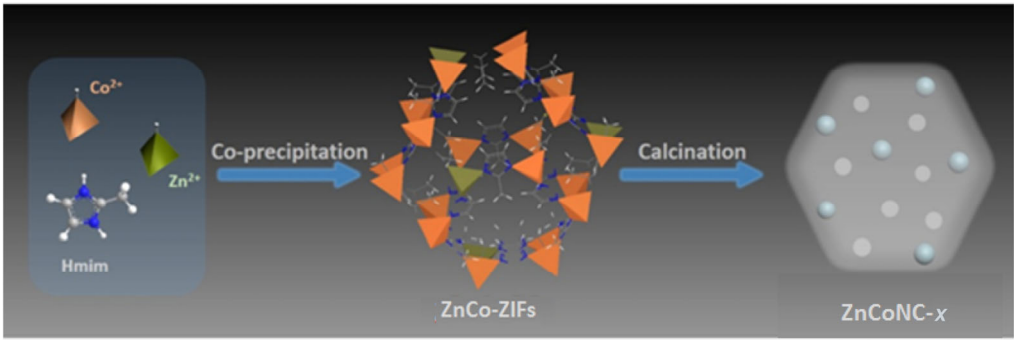

Figure 1 Schematic illustration of the synthesis of ZnCoNC-*x* using ZnCo-ZIFs as templates.

ZnCoNC materials with better ORR and OER catalytic activity under alkaline conditions, compared to their Zn-free counterparts (CoNC). The ZnCoNC-0.1 sample was found to exhibit the best ORR and OER performance, even superior to that of the commercial Pt/C and Ru/C catalysts. The high catalytic activity of this sample could be attributed to the synergistic effect of N-doped carbon and Co nanoparticles in the composite, as well as to its high nitrogen content, its improved conductivity resulting from the high graphitization of carbon, and its large surface area associated with the porous polyhedral structure. A primary zinc-air battery fabricated with the ZnCoNC-0.1 catalyst as cathode showed a specific capacity of 741 $mAh \cdot g_{Zn}^{-1}$ at a current density of 7 $mA \cdot cm^{-2}$. Furthermore, lower charge and discharge voltages were recorded for the rechargeable Zn-air battery based on the ZnCoNC-0.1 than on the Pt/C catalyst, under the same test conditions.

2 Experimental

2.1 Synthesis of Zn-doped Co-based ZIFs (ZnCo-ZIFs)

All chemicals and solvents were purchased from commercial sources and used without further purification. The synthesis of ZnCo-ZIF nanocrystals was based on a previously reported procedure, with some modifications [32]. Typically, a mixture of $Co(NO_3)_2 \cdot 6H_2O$ and $Zn(NO_3)_2 \cdot 6H_2O$ (3 mmol in total) with the desired Zn^{2+}/Co^{2+} molar ratio was dissolved in 25 mL of methanol to form a clear solution, which was subsequently poured into 25 mL of methanol containing 4 mmol of 2-methylimidazole. After vigorous stirring for 5 min, the resulting solution was incubated at room temperature for 24 h. The product was separated by centrifugation, thoroughly washed several times with ethanol, and finally dried overnight at 50 °C. We prepared a series of ZnCo-ZIFs with different Zn/Co ratios, denoted as ZnCo-ZIF-x (where x is the Zn/Co ratio).

2.2 Synthesis of porous carbon polyhedra from ZnCo-ZIFs

Porous carbon polyhedra were prepared by a thermolysis method. Typically, a powdered ZnCo-ZIF sample was placed in a tube furnace, heated at 1 °C·min^{-1}, and carbonized at 500 °C for 2 h under nitrogen gas flow. The product was then cooled to room temperature naturally, until its color changed from pink to black. The obtained porous carbon materials were labeled as ZnCoNC-x (where x denotes the Zn/Co ratio in the original ZnCo-ZIFs).

2.3 Materials characterization

The phase purity of all products was characterized by powder X-ray diffraction (XRD, Bruker AXS D8) with Cu Kα radiation (λ = 1.5406 Å). The morphology, structure, and composition of the samples were characterized by field-emission scanning electron microscopy (SEM, Zeiss SUPRA 55) operating at 20 kV, transmission electron microscopy (TEM, FEI Tecnai G2 20 S-Twin), and high-resolution transmission electron microscopy (HRTEM). The latter was performed with a JEOL JEM 2100 spectrometer equipped with an energy-dispersive X-ray spectrometry (EDS) instrument operating at 200 kV. Thermogravimetric analysis measurements were carried out on a Q500 (TA Instruments) thermoanalyzer with a heating rate of 10 °C·min^{-1} under nitrogen atmosphere. Chemical compositions were determined by elemental analysis (Elementar Vario EL cube V2.0.1) and X-ray photoelectron spectroscopy (XPS) (Thermo Electron ESCALAB 250).

2.4 Electrochemical measurements

The ORR and OER electrochemical activities of the catalysts were evaluated in a standard three-electrode system using a PARSTAT 2273 potentiostat workstation (Princeton Applied Research) in a 0.1 M KOH electrolyte. The working electrodes were prepared by dispersing 5 mg of catalyst in 0.5 mL absolute ethanol, and then adding 10 μL of 5% Nafion (DuPont) under sonication to form a homogeneous ink. Finally, the catalyst (6 μL, or ~ 60 μg) was drop-casted onto a glassy carbon rotating disk electrode (diameter 5 mm) to achieve a loading amount of 0.2 mg·cm^{-2}. Pt and Ag/AgCl (with a saturated KCl solution) were employed as counter and reference electrodes, respectively. All potentials reported in this work are relative to the reversible hydrogen electrode (RHE). The ORR catalytic activity

was evaluated from 0.1 to 1.0 V vs. RHE, whereas the OER catalytic performance was measured from 1.1 to 1.9 V vs. RHE.

2.5 Zinc-air battery fabrication and testing

A home-made zinc-air cell device was designed for the battery test. The air cathodes were prepared by the following procedure: The catalyst (2.0 mg), activated carbon (0.8 mg), and polytetrafluoroethylene (PTFE, 10 μL) were dispersed in 10 mL of ethanol, while another mixture was prepared by dispersing activated carbon (4.0 mg), carbon black (0.8 mg), and PTFE (30 μL) in 1 mL of ethanol. The two resulting mixtures were then sonicated to form homogeneous inks. Ni foams were carefully washed with a 1 M HCl solution and then rinsed with absolute ethanol and distilled water. The two inks were carefully dropped onto the Ni foam and kept in a vacuum container for 30 min, followed by pressing the two resulting Ni foams together. A 6 M KOH solution and a polished zinc plate were used as electrolyte and anode, respectively, of the zinc-air battery. Battery testing and cycling experiments were performed at 25 ℃ using the recurrent galvanic pulse method, with one cycle consisting of a discharging step (7 mg·cm^{-2} for 10 min) followed by a charging step of the same current and duration.

3 Results and discussion

The synthetic route for the preparation of ZnCoNC-x materials based on the bimetallic ZIF templates is illustrated in Fig. 1. First, bimetallic ZIFs with a unique polyhedral morphology were prepared by reacting a mixture of $Zn(NO_3)_2$ and $Co(NO_3)_2$ with 2-methylimidazole in methanol at room temperature. Then, N-doped porous carbon polyhedra containing uniformly distributed metal and bimetallic oxide (Co, $Zn_xCo_{3-x}O_4$ and/or Co_3O_4) nanoparticles were readily obtained through a thermally-induced decomposition process.

The morphology and composition of the ZnCo-ZIFs were first examined by SEM and XRD. As shown in the SEM images of Figs. 2(a) and 2(b), the ZnCo-ZIFs particles have good uniformity, with a size of 1 μm and a regular rhombic dodecahedral crystal structure. The powder XRD patterns (Fig. 2(c)) of the ZnCo-ZIFs confirm their high crystallinity and zeolite-type structure. The as-prepared ZnCo-ZIFs were then heated under N_2 gas flow at 500 ℃ at a heating rate of 1 ℃·min^{-1} to obtain the ZnCoNC-x materials. This extremely low heating rate served to preserve the framework of ZIFs, because the carbon generated during this process acts as a temporal buffer, preventing further contraction of the ZIFs. The SEM images of the obtained ZnCoNC-0.1 catalyst (Figs. 2(d) and 2(e)) show that the particle size was reduced to approximately 500 nm and retained the rhombic dodecahedral morphology of the ZnCo-ZIF precursors, with a slight surface shrinkage due to the decomposition process. The different Zn/Co molar ratios did not influence the morphology and phase structure of the ZnCoNC-x materials, as shown in Figs. 2(d) and 2(e), and Figs. S1(a)–S1(h) in the Electronic Supplementary Material (ESM). The crystallographic structure and phase composition of CoNC and ZnCoNC-0.1 were determined by XRD (Fig. 2(f)). The XRD patterns of the two samples exhibited a broad peak at approximately 26°, which can be indexed to the (002) reflection of graphitic carbon (powder diffraction file (PDF) 26-1077). The intense peaks located at around 44° and 51° could be assigned to the (111) and (220) reflections of face-centered cubic (fcc) Co (PDF 15-0806), indicating that metal Co was formed during the pyrolysis process. Moreover, the XRD pattern of CoNC exhibited a peak at 2θ= 36° that could be associated to the (311) planes of spinel Co_3O_4 (PDF 42-1467). In the case of the ZnCoNC-0.1 samples, the peak slightly shifted to lower angles, suggesting that incorporation of Zn^{2+} into the Co_3O_4 lattice resulted in the formation of a solid solution of $Zn_xCo_{3-x}O_4$ [34]. The TEM images of ZnCoNC-0.1 (Fig. 2(g)) show that small nanoparticles with a size of about 8–15 nm were encapsulated within the carbon shell.

The fine structure of the nanoparticles was analyzed by HRTEM analysis, and the results are shown in Fig. 2(h). The Co nanoparticles and the graphitic carbon shell showed clear lattice spacings of 0.205 and 0.351 nm, respectively, which match well with the Co (111) and C (002) planes, respectively. The EDS analysis of the ZnCoNC-0.1 sample reveal the presence of Zn, Co, N, and C elements (Fig. 2(i)). The TEM

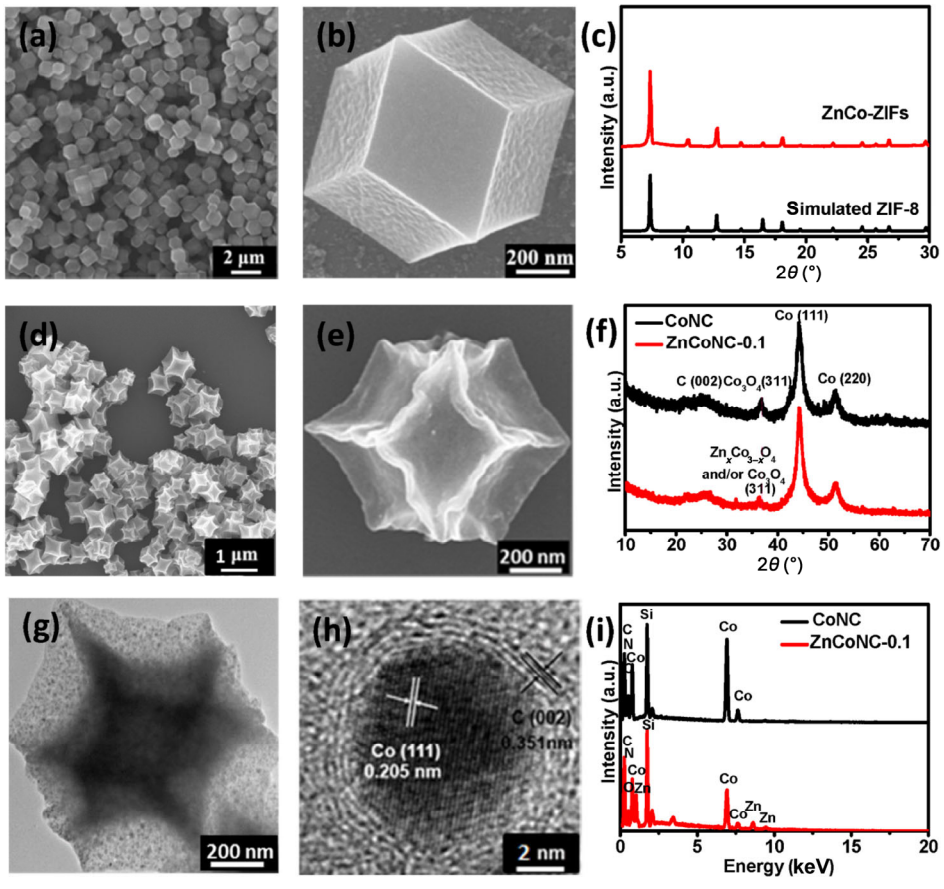

Figure 2 (a) and (b) SEM images and (c) XRD patterns of the prepared ZnCo-ZIFs; (d) and (e) SEM, (g) TEM, and (h) HRTEM images of ZnCoNC-0.1; (f) XRD patterns and (i) EDS spectrum of CoNC and ZnCoNC-0.1.

images (Figs. S2(a) and S2(b) in the ESM) show that, after being uniformly embedded in the porous ZnCoNC-0.1 matrix, the Co particles exhibit an average diameter of 10.38 nm, which is smaller than that of the Co particles in CoNC (11.64 nm). This result clearly demonstrates that the presence of Zn species could effectively modulate the Co nanoparticle size by suppressing sintering upon spatially isolating Co from Zn species [35]. The N_2 adsorption–desorption isotherms of CoNC and ZnCoNC-0.1 are shown in Fig. S3 of the ESM. ZnCoNC-0.1 showed a specific surface area of 502.7 $m^2 \cdot g^{-1}$, much larger than that of CoNC (156.6 $m^2 \cdot g^{-1}$), indicating that Zn doping leads to a larger specific area.

XPS analysis was used to investigate the chemical composition and bonding state of the elements in ZnCoNC-0.1. The full XPS spectra (Fig. 3(a)) of CoNC and ZnCoNC-0.1 reveal the presence of carbon, cobalt, nitrogen, and oxygen species. Compared to CoNC, the nitrogen content in ZnCoNC-0.1 increased from 1.34 at.% to 6.33 at.%, suggesting that Zn doping in porous carbon polyhedra results in a higher nitrogen content. The XPS spectra of ZnCoNC-0.1 are shown in Figs. 3(b)–3(f). The high-resolution N 1s spectrum (Fig. 3(b)) reveals three types of nitrogen species: graphitic (400.1 eV), pyrrolic (398.1 eV), and pyridinic N (398.8 eV). It has been reported that these species play an important role in the ORR and OER processes [32, 36, 37], where pyridinic N could improve the onset potential, while graphitic N determines the limiting current for ORR [11]. The total content of pyridinic, pyrrolic, and graphitic N in ZnCoNC-0.1 was much higher than that measured for CoNC, which further promotes the ORR and OER activity of ZnCoNC-0.1. The C 1s peaks in Fig. 3(c) can be decomposed into three individual peaks with binding energies of 284.6, 286.5, and 288.7 eV, respectively attributed to the sp^2 carbon, C–O, and C=O/C=N groups in the ZnCoNC-0.1

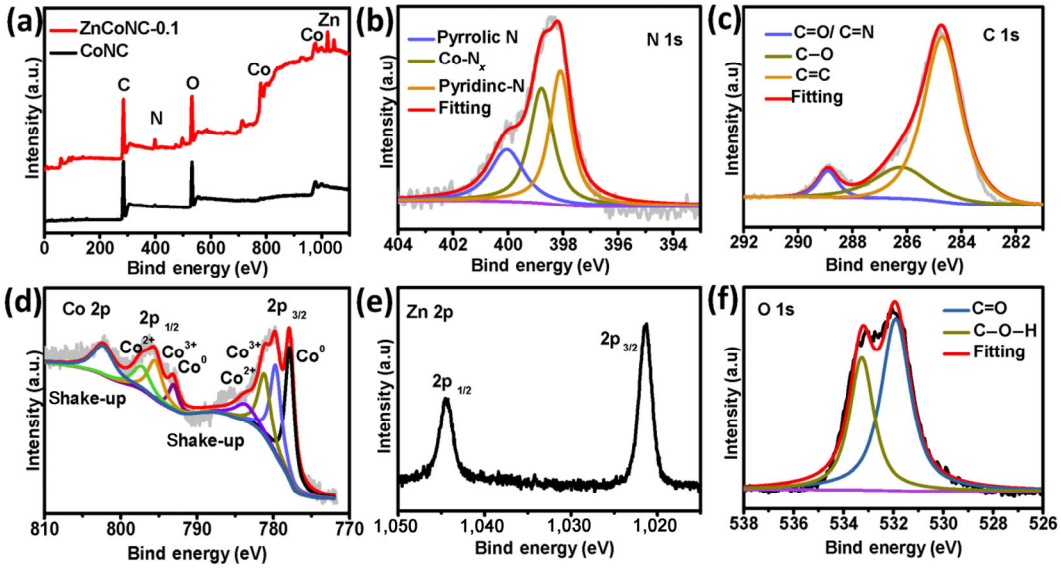

Figure 3 (a) Full XPS spectra of CoNC and ZnCoNC-0.1. (b) N 1s, (c) C 1s, (d) Co 2p, (e) Zn 2p, and (f) O 1s spectra of ZnCoNC-0.1.

sample [38]. The decomposition of the Co 2p spectrum in the Co^{3+}, Co^{2+}, and Co^{0} contributions is shown in Fig. 3(d). The characteristic peaks at 779.8 and 781.3 eV can be attributed to $Co^{3+}{}_{3/2}$ and $Co^{2+}{}_{3/2}$, respectively. The other spin-orbit component, $2p_{1/2}$, appears at 795.6 and 797.4 eV for Co^{3+} and Co^{2+}, respectively. The components at 777.8 and 793.15 eV correspond to metallic Co [39, 40]. Compared to CoNC, a negative shift of the Co 2p peaks was observed for the ZnCoNC-0.1 sample, probably due to the incorporation of Zn^{2+} (Fig. S4 in the ESM), which is expected to enhance the OER activity of the catalyst [34, 41]. Moreover, the signals at binding energies of 1,044.2 and 1,020.8 eV were assigned to Zn $2p_{3/2}$ and Zn $2p_{1/2}$ (Fig. 3(e)) [34], whereas the high-resolution O 1s spectrum could be fitted by two peaks at 533.3 and 531.9 eV, which correspond to C–O–H and C=O groups [42], respectively (Fig. 3(f)).

The electrocatalytic ORR and OER activities of the as-prepared materials were initially evaluated in a three-electrode electrochemical cell by linear sweep voltammetry (LSV) with a rotating ring-disk electrode (RRDE) as the working electrode.

To evaluate the ORR performances, Fig. 4(a) shows the polarization curves (not corrected for internal resistance) of electrodes coated with ZnCoNC-*x* and commercial Pt/C catalysts, measured in O_2-saturated 0.1 M KOH electrolyte under a rotation rate of 1,600 rpm. The ZnCoNC-0.1 sample exhibited a half-wave potential of 0.84 V, higher than that of commercial Pt/C electrodes (0.81 V), and also much better than that of CoNC (0.80 V), ZnCoNC-0.05 (0.82 V), ZnCoNC-0.13 (0.75 V), and ZnCoNC-0.2 (0.67 V), indicating that the lowest ORR overpotential is obtained in the case of ZnCoNC-0.1. ZnCoNC-0.1 also exhibited a more positive onset potential (0.9 V) toward ORR compared to other catalysts, including commercial Pt/C (whose onset potential was 0.89 V), indicating a better intrinsically thermodynamic catalytic capability. The excellent ORR activity of the ZnCoNC-0.1 catalyst was further confirmed by its significantly smaller Tafel slope of 66 $mV \cdot dec^{-1}$ compared to commercial Pt/C (72 $mV \cdot dec^{-1}$) and ZnCoNC-*x* catalysts (85 $mV \cdot dec^{-1}$ for CoNC, 70 $mV \cdot dec^{-1}$ for ZnCoNC-0.05, 77 $mV \cdot dec^{-1}$ for ZnCoNC-0.13, and 83 $mV \cdot dec^{-1}$ for ZnCoNC-0.2) (Fig. 4(b)). The different ORR performance of CoNC and ZnCoNC-*x* highlights the benefits of Zn addition to the MOF-derived catalysts. In particular, Zn doping allowed us to optimize the Co nanoparticle size, the pyridinic and pyrrolic N contents, and hence the ORR activity. The durabilities of ZnCoNC-0.1 and Pt/C were evaluated using chronoamperometric measurements at 0.8 V (vs. RHE) in O_2-saturated 0.1 M KOH solution, performed with a rotation rate of 1600 rpm for 10,000 s (Fig. S5(a) in the ESM). The Pt/C catalyst shows a 31% decrease in activity after 10,000 s.

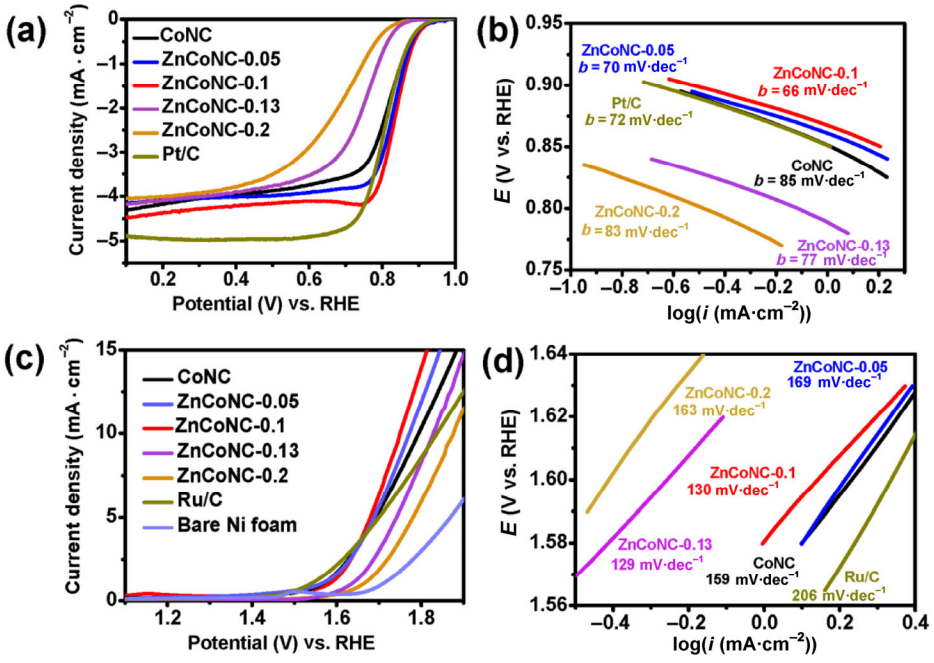

Figure 4 Electrochemical performance of ZnCoNC-*x*. (a) Polarization curves (not corrected for internal resistance) of ZnCoNC-*x* and Pt/C from 1.0 to 0.1 V (vs. RHE) in O_2-saturated 0.1 M KOH at a sweep rate of 5 mV·s^{-1} and 1,600 rpm; (b) corresponding Tafel plots. (c) Polarization curves (not corrected for internal resistance) of ZnCoNC-*x*, Ru/C, and Ni foam from 1.1 to 1.9 V (vs. RHE) in O_2-saturated 0.1 M KOH at a sweep rate of 5 mV·s^{-1} and 1,600 rpm; (d) corresponding Tafel plots.

As a comparison, ZnCoNC-0.1 retains a high relative current of 80% after the same time, indicating its superior stability in an alkaline environment. Apart from the ORR activity, a high OER activity is another critical requirement for bifunctional catalysts used in metal-air batteries. The polarization curves (not corrected for internal resistance) of ZnCoNC-*x*, commercial Ru/C catalysts, and Ni foam were recorded from 1.1 to 1.9 V (vs. RHE) at a scan rate of 5 mV·s^{-1} in O_2-saturated 0.1 M KOH solution. As shown in Fig. 4(c), the ZnCoNC-0.1 catalyst showed a significantly lower potential (1.75 V) at a current density of 10 mA·cm^{-2} compared to commercial Ru/C (1.83 V), CoNC (1.79 V), ZnCoNC-0.05 (1.77 V), ZnCoNC-0.13 (1.82 V), and ZnCoNC-0.2 (1.87 V). The potential contribution of Ni foam can be ruled out, based on the high overpotential measured in the LSV test on bare Ni foam. Moreover, Fig. 4(d) shows that ZnCoNC-0.1 exhibited a much lower Tafel slope (129 mV·dec^{-1}) than CoNC (159 mV·dec^{-1}), ZnCoNC-0.05 (169 mV·dec^{-1}), ZnCoNC-0.13 (130 mV·dec^{-1}), ZnCoNC-0.2 (162 mV·dec^{-1}), and commercial Ru/C (206 mV·dec^{-1}), further confirming the superior OER performance of ZnCoNC-0.1. The durabilities of ZnCoNC-0.1 and Ru/C were evaluated using chronoamperometric measurements. The current–time (*i*–*t*) curve highlights the high stability of ZnCoNC-0.1 (Fig. S5(b) in the ESM), which retains more than 93.1% of the initial current after 10,000 s. In contrast, the Ru/C catalyst suffers from a rapid current loss with only 74.5% retention and shows a 25.5% decrease in activity after 10,000 s. Inductively coupled plasma (ICP) measurements revealed that the Zn content of ZnCoNC-0.1 decreased from 12.6% to 4% after the OER durability test, indicating that a fraction of Zn species reacted with the KOH electrolyte during testing. The improved ORR and OER activities of ZnCoNC-0.1 can be attributed to its large specific surface area, good dispersion of Co nanoparticles, and high N content. It has been reported that Zn doping could effectively modulate the Co nanoparticle size, by suppressing sintering through the spatial isolation of Co by Zn species. A smaller Co nanoparticle size could enhance the interaction between Co and coordinated N, leading to a higher N content. The incorporation of small well-dispersed Co nanoparticles in the porous carbon matrix and the

high N content can reduce the energy barrier for O_2 adsorption and accelerate the rate-limiting first electron transfer step of the ORR process. The large surface area of ZnCoNC-0.1 will increase the accessibility of ORR and OER active sites, thus resulting in superior electrocatalytic ORR and OER activity. The XPS analysis showed that the incorporation of Zn^{2+} in the CoNC matrix leads to a negative shift of the Co 2p peaks, which is considered beneficial for the enhancement of the OER activity of the catalyst. Therefore, Zn doping improved the catalytic activity of CoNC in both ORR and OER processes, with ZnCoNC-0.1 exhibiting the highest catalytic activity.

Apart from the standard electrochemical tests in aqueous electrolytes described above, a prototype of a two-electrode zinc-air cell was assembled to further examine the bifunctional catalytic performance of the present materials under real battery operation conditions. The best ORR and OER catalyst identified in the electrochemical tests, ZnCoNC-0.1, was used as a cathode to evaluate its performance in zinc-air batteries. During deep discharge of the cell, i.e., until complete consumption of the Zn metal at a constant current density of 7 mA·cm^{-2}, the open-circuit potential was 1.28 V, followed by the average working voltage plateau at approximately 1.24 V (Fig. 5(a)). The corresponding discharge capacity (normalized to the mass of consumed Zn) was found to be 741 mAh·g_{Zn}^{-1}, corresponding to a gravimetric energy density of 889 Wh·g_{Zn}^{-1}, and significantly higher than the capacity of a Pt/C based battery (540 mAh·g_{Zn}^{-1}). A discharge/charge experiment was performed with a current rate of 7 mA·cm^{-2}, as shown in Fig. 5(b). The initial charge and discharge potentials of ZnCoNC-0.1 were close to 2.03 and 1.19 V, respectively; after 33 h, the corresponding final values were 2.04 and 1.19 V. This exceptional performance is superior to that of commercial Pt/C and many other transition metal- and/or carbon-based zinc-air batteries, as shown in Table 1. This result highlights the good cycling stability of the ZnCoNC-0.1 catalyst in the discharge and charge processes.

Table 1 Comparison of the electrochemical performances of discharged/charged zinc-air batteries fabricated with various air catalysts (electrolyte: 6 M KOH)

Air catalysts	Current density (mA·cm^{-2})	Number of cycle	Increased polarization[a] (V)	Ref.
MnO_2/Co_3O_4	15	60	0.3	[43]
MnO_2-NCNT	8	50	0.4	[44]
$NiCo_2O_4$	25	50	0.2	[45]
$LaNiO_3$/NCNT	17.6	75	0.1–0.2	[46]
BNPC	2	600	0.1	[47]
ZnCoNC-0.1	7	100	0.01	This work

[a]Polarization refers to the difference between charge and discharge voltages at the same working current density.

4 Conclusions

In summary, ZnCoNC-x materials with active CoN_x, $Zn_xCo_{3-x}O_4$, and/or Co_3O_4 sites, high graphitization, as well as a porous polyhedral structure with large surface area, have been designed and successfully

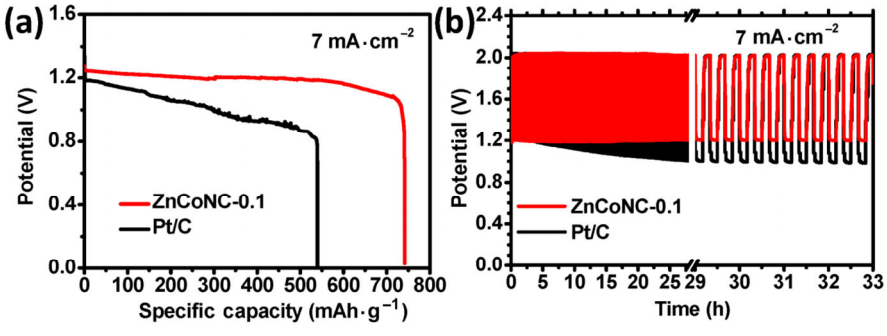

Figure 5 Electrochemical performances of zinc-air batteries fabricated using ZnCoNC-0.1 and Pt/C as catalysts in 6 M KOH. (a) Typical discharge curves of primary Zn-air batteries under continuous discharge until complete consumption of Zn at a current density of 7 mA·cm^{-2}. The specific capacity was normalized to the mass of consumed Zn. (b) Discharge/charge cycling curves of rechargeable zinc-air batteries at a current density of 7 mA·cm^{-2}.

synthesized using bimetallic MOFs as templates/precursors. Outstanding ORR and OER activities were measured for the ZnCoNC-0.1 sample and interpreted in terms of the synergistic effect of N-doped carbon and Co nanoparticles in the composite, high nitrogen content, improved conductivity deriving from the high graphitization of carbon, and large surface area associated with the porous polyhedral structure. Zn doping also resulted in a smaller Co nanoparticle size and higher nitrogen contents, which further promote the ORR and OER activity. The optimized ZnCoNC-0.1 sample exhibits excellent ORR and OER activities, along with good performance in primary and rechargeable zinc-air batteries. The facile route to fabricate porous carbon hybrids illustrated here may be extended to other catalysts and electrode materials for fuel cells, metal-air batteries, and water splitting applications.

Acknowledgements

This work was financially supported by the National Natural Science Foundation of China, Beijing Engineering Center for Hierarchical Catalysts, the Fundamental Research Funds for the Central Universities (No. YS1406), Program for Changjiang Scholars and Innovative Research Team in University, and the National Basic Research Program of China (No. 2014CB932104).

Electronic Supplementary Material: Supplementary material (SEM, TEM, XPS) is available in the online version of this article at https://doi.org/10.1007/s12274-017-1615-2.

References

[1] Aricò, A. S.; Bruce, P.; Scrosati, B.; Tarascon, J. M.; van Schalkwijk, W. Nanostructured materials for advanced energy conversion and storage devices. *Nat. Mater.* **2005**, *4*, 366–377.

[2] Girishkumar, G.; McCloskey, B.; Luntz, A. C.; Swanson, S.; Wilcke, W. Lithium-air battery: Promise and challenges. *J. Phys. Chem. Lett.* **2010**, *1*, 2193–2203.

[3] Lee, J. S.; Tai Kim, S.; Cao, R. G.; Choi, N. S.; Liu, M. L.; Lee, K. T.; Cho, J. Metal-air batteries with high energy density: Li-air versus Zn-air. *Adv. Energy Mater.* **2011**, *1*, 34–50.

[4] Wang, H. G.; Zhang, X. B. Designing multi-shelled metal oxides: Towards high energy-density lithium-ion batteries. *Sci. China Mater.* **2016**, *59*, 521–522.

[5] Li, Y. G.; Dai, H. J. Recent advances in zinc-air batteries. *Chem. Soc. Rev.* **2014**, *43*, 5257–5275.

[6] Zhu, A. L.; Wilkinson, D. P.; Zhang, X.; Xing, Y. L.; Rozhin, A. G.; Kulinich, S. A. Zinc regeneration in rechargeable zinc-air fuel cells—A review. *J. Energy Storage* **2016**, *8*, 35–50.

[7] Liu, Q.; Wang, Y. B.; Dai, L. M.; Yao, J. N. Scalable fabrication of nanoporous carbon fiber films as bifunctional catalytic electrodes for flexible Zn-air batteries. *Adv. Mater.* **2016**, *28*, 3000–3006.

[8] Zang, Y. P.; Zhang, H. M.; Zhang, X.; Liu, R. R.; Liu, S. W.; Wang, G. Z.; Zhang, Y. X.; Zhao, H. J. Fe/Fe_2O_3 nanoparticles anchored on Fe-N-doped carbon nanosheets as bifunctional oxygen electrocatalysts for rechargeable zinc-air batteries. *Nano Res.* **2016**, *9*, 2123–2137.

[9] Li, X. Z.; Fang, Y. Y.; Lin, X. Q.; Tian, M.; An, X. C.; Fu, Y.; Li, R.; Jin, J.; Ma, J. T. MOF derived Co_3O_4 nanoparticles embedded in N-doped mesoporous carbon layer/MWCNT hybrids: Extraordinary bi-functional electrocatalysts for OER and ORR. *J. Mater. Chem. A* **2015**, *3*, 17392–17402.

[10] Liang, Y. Y.; Li, Y. G.; Wang, H. L.; Zhou, J. G.; Wang, J.; Regier, T.; Dai, H. J. Co_3O_4 nanocrystals on graphene as a synergistic catalyst for oxygen reduction reaction. *Nat. Mater.* **2011**, *10*, 780–786.

[11] Su, Y. H.; Zhu, Y. H.; Jiang, H. L.; Shen, J. H.; Yang, X. L.; Zou, W. J.; Chen, J. D.; Li, C. Z. Cobalt nanoparticles embedded in N-doped carbon as an efficient bifunctional electrocatalyst for oxygen reduction and evolution reactions. *Nanoscale* **2014**, *6*, 15080–15089.

[12] Yang, Q.; Liu, W. X.; Wang, B. Q.; Zhang, W. N.; Zeng, X. Q.; Zhang, C.; Qin, Y. J.; Sun, X. M.; Wu, T. P.; Liu, J. F. et al. Regulating the spatial distribution of metal nanoparticles within metal-organic frameworks to enhance catalytic efficiency. *Nat. Commun.* **2017**, *8*, 14429.

[13] Zhang, Z. C.; Chen, Y. F.; Xu, X. B.; Zhang, J. C.; Xiang, G. L.; He, W.; Wang, X. Well-defined metal-organic framework hollow nanocages. *Angew. Chem., Int. Ed.* **2014**, *53*, 429–433.

[14] Zhang, Z. C.; Chen, Y. F.; He, S.; Zhang, J. C.; Xu, X. B.; Yang, Y.; Nosheen, F.; Saleem, F.; He, W.; Wang, X. Hierarchical Zn/Ni-MOF-2 nanosheet-assembled hollow nanocubes for multicomponent catalytic reactions. *Angew. Chem.* **2014**, *126*, 12725–12729.

[15] Zhang, W. N.; Lu, G.; Cui, C. L.; Liu, Y. Y.; Li, S. Z.; Yan, W. J.; Xing, C.; Chi, Y. R.; Yang, Y. H.; Huo, F. W. A

family of metal-organic frameworks exhibiting size-selective catalysis with encapsulated noble-metal nanoparticles. *Adv. Mater.* **2014**, *26*, 4056–4060.

[16] Lu, G.; Li, S. Z.; Guo, Z.; Farha, O. K.; Hauser, B. G.; Qi, X. Y.; Wang, Y.; Wang, X.; Han, S. Y.; Liu, X. G. et al. Imparting functionality to a metal-organic framework material by controlled nanoparticle encapsulation. *Nat. Chem.* **2012**, *4*, 310–316.

[17] Li, Z.; Yu, R.; Huang, J. L.; Shi, Y. S.; Zhang, D. Y.; Zhong, X. Y.; Wang, D. S.; Wu, Y. E.; Li, Y. D. Platinum-nickel frame within metal-organic framework fabricated *in situ* for hydrogen enrichment and molecular sieving. *Nat. Commun.* **2015**, *6*, 8248.

[18] Liu, W. X.; Huang, J. J.; Yang, Q.; Wang, S. J.; Sun, X. M.; Zhang, W. N.; Liu, J. F.; Huo, F. W. Multi-shelled hollow metal-organic frameworks. *Angew. Chem.* **2017**, *56*, 5512–5516.

[19] Wu, R. B.; Qian, X. K.; Zhou, K.; Wei, J.; Lou, J.; Ajayan, P. M. Porous spinel $Zn_xCo_{3-x}O_4$ hollow polyhedra templated for high-rate lithium-ion batteries. *ACS Nano* **2014**, *8*, 6297–6303.

[20] Xu, X. D.; Cao, R. G.; Jeong, S.; Cho, J. Spindle-like mesoporous α-Fe_2O_3 anode material prepared from MOF template for high-rate lithium batteries. *Nano Lett.* **2012**, *12*, 4988–4991.

[21] Kim, T. K.; Lee, K. J.; Cheon, J. Y.; Lee, J. H.; Joo, S. H.; Moon, H. R. Nanoporous metal oxides with tunable and nanocrystalline frameworks via conversion of metal-organic frameworks. *J. Am. Chem. Soc.* **2013**, *135*, 8940–8946.

[22] Jiao, L.; Zhou, Y. X.; Jiang, H.-L. Metal-organic framework-based CoP/reduced graphene oxide: High-performance bifunctional electrocatalyst for overall water splitting. *Chem. Sci.* **2016**, *7*, 1690–1695.

[23] Zhang, P.; Sun, F.; Xiang, Z. H.; Shen, Z. G.; Yun, J.; Cao, D. P. ZIF-derived *in situ* nitrogen-doped porous carbons as efficient metal-free electrocatalysts for oxygen reduction reaction. *Energy Environ. Sci.* **2014**, *7*, 442–450.

[24] Pandiaraj, S.; Aiyappa, H. B.; Banerjee, R.; Kurungot, S. Post modification of MOF derived carbon via g-C_3N_4 entrapment for an efficient metal-free oxygen reduction reaction. *Chem. Commun.* **2014**, *50*, 3363–3366.

[25] Chaikittisilp, W.; Ariga, K.; Yamauchi, Y. A new family of carbon materials: Synthesis of MOF-derived nanoporous carbons and their promising applications. *J. Mater. Chem. A* **2013**, *1*, 14–19.

[26] Ma, T. Y.; Dai, S.; Jaroniec, M.; Qiao, S. Z. Metal-organic framework derived hybrid Co_3O_4-carbon porous nanowire arrays as reversible oxygen evolution electrodes. *J. Am. Chem. Soc.* **2014**, *136*, 13925–13931.

[27] Hou, Y.; Huang, T. Z.; Wen, Z. H.; Mao, S.; Cui, S. M.; Chen, J. H. Metal-organic framework-derived nitrogen-doped core-shell-structured porous Fe/Fe_3C@C nanoboxes supported on graphene sheets for efficient oxygen reduction reactions. *Adv. Energy Mater.* **2014**, *4*, 1400337.

[28] Xia, W.; Zou, R. Q.; An, L.; Xia, D. G.; Guo, S. J. A metal–organic framework route to *in situ* encapsulation of Co@Co_3O_4@C core@bishell nanoparticles into a highly ordered porous carbon matrix for oxygen reduction. *Energy Environ. Sci.* **2015**, *8*, 568–576.

[29] Zhang, T. Y.; Liu, W. X.; Meng, G.; Yang, Q.; Sun, X. M.; Liu, J. F. Construction of hierarchical copper-based metal-organic framework nanoarrays as functional structured catalysts. *ChemCatChem* **2017**, *9*, 1771–1775.

[30] Li, J. S.; Chen, Y. Y.; Tang, Y. J.; Li, S. L.; Dong, H. Q.; Li, K.; Han, M.; Lan, Y.-Q.; Bao, J. C.; Dai, Z. H. Metal-organic framework templated nitrogen and sulfur co-doped porous carbons as highly efficient metal-free electrocatalysts for oxygen reduction reactions. *J. Mater. Chem. A* **2014**, *2*, 6316–6319.

[31] Yin, P. Q.; Yao, T.; Wu, Y. E.; Zheng, L. R.; Lin, Y.; Liu, W.; Ju, H. X.; Zhu, J. F.; Hong, X.; Deng, Z. X. et al. Single cobalt atoms with precise N-coordination as superior oxygen reduction reaction catalysts. *Angew. Chem., Int. Ed.* **2016**, *55*, 10800–10805.

[32] Chen, Y.-Z.; Wang, C. M.; Wu, Z.-Y.; Xiong, Y. J.; Xu, Q.; Yu, S.-H.; Jiang, H.-L. From bimetallic metal-organic framework to porous carbon: High surface area and multicomponent active dopants for excellent electrocatalysis. *Adv. Mater.* **2015**, *27*, 5010–5016.

[33] Xia, B. Y.; Yan, Y.; Li, N.; Wu, H. B.; Lou, X. W.; Wang, X. A metal-organic framework-derived bifunctional oxygen electrocatalyst. *Nat. Energy* **2016**, *1*, 15006.

[34] Liu, X. J.; Chang, Z.; Luo, L.; Xu, T. H.; Lei, X. D.; Liu, J. F.; Sun, X. M. Hierarchical $Zn_xCo_{3-x}O_4$ nanoarrays with high activity for electrocatalytic oxygen evolution. *Chem. Mater.* **2014**, *26*, 1889–1895.

[35] You, B.; Jiang, N.; Sheng, M. L.; Drisdell, W. S.; Yano, J.; Sun, Y. J. Bimetal-organic framework self-adjusted synthesis of support-free nonprecious electrocatalysts for efficient oxygen reduction. *ACS Catal.* **2015**, *5*, 7068–7076.

[36] Chen, B. L.; Li, R.; Ma, G. P.; Gou, X. L.; Zhu, Y. Q.; Xia, Y. D. Cobalt sulfide/N,S codoped porous carbon core-shell nanocomposites as superior bifunctional electrocatalysts for oxygen reduction and evolution reactions. *Nanoscale* **2015**, *7*, 20674–20684.

[37] Han, Y. J.; Zhai, J. F.; Zhang, L. L.; Dong, S. J. Direct carbonization of cobalt-doped NH_2-MIL-53(Fe) for electrocatalysis of oxygen evolution reaction. *Nanoscale* **2016**, *8*,

1033–1039.

[38] Zhang, G. J.; Li, C. X.; Liu, J.; Zhou, L.; Liu, R. H.; Han, X.; Huang, H.; Hu, H. L.; Liu, Y.; Kang, Z. H. One-step conversion from metal-organic frameworks to Co_3O_4@N-doped carbon nanocomposites towards highly efficient oxygen reduction catalysts. *J. Mater. Chem. A* **2014**, *2*, 8184–8189.

[39] Meng, G.; Yang, Q.; Wang, Y. X.; Sun, X. M.; Liu, J. F. NiCoFe spinel-type oxide nanosheet arrays derived from layered double hydroxides as structured catalysts. *RSC Adv.* **2014**, *4*, 57804–57809.

[40] Liu, X. J.; Liu, J. F.; Sun, X. M. $NiCo_2O_4$@NiO hybrid arrays with improved electrochemical performance for pseudocapacitors. *J. Mater. Chem. A* **2015**, *3*, 13900–13905.

[41] Zhang, Y.; Cui, B.; Qin, Z. T.; Lin, H.; Li, J. B. Hierarchical wreath-like Au-$Co(OH)_2$ microclusters for water oxidation at neutral pH. *Nanoscale* **2013**, *5*, 6826–6833.

[42] Mattevi, C.; Eda, G.; Agnoli, S.; Miller, S.; Mkhoyan, K. A.; Celik, O.; Mastrogiovanni, D.; Granozzi, G.; Garfunkel, E.; Chhowalla, M. Evolution of electrical, chemical, and structural properties of transparent and conducting chemically derived graphene thin films. *Adv. Funct. Mater.* **2009**, *19*, 2577–2583.

[43] Du, G. J.; Liu, X. G.; Zong, Y.; Hor, T. S. A.; Yu, A. S.; Liu, Z. L. Co_3O_4 nanoparticle-modified MnO_2 nanotube bifunctional oxygen cathode catalysts for rechargeable zinc-air batteries. *Nanoscale* **2013**, *5*, 4657–4661.

[44] Chen, Z.; Yu, A. P.; Ahmed, R.; Wang, H. J.; Li, H.; Chen, Z. W. Manganese dioxide nanotube and nitrogen-doped carbon nanotube based composite bifunctional catalyst for rechargeable zinc-air battery. *Electrochim. Acta* **2012**, *69*, 295–300.

[45] Prabu, M.; Ketpang, K.; Shanmugam, S. Hierarchical nanostructured $NiCo_2O_4$ as an efficient bifunctional non-precious metal catalyst for rechargeable zinc-air batteries. *Nanoscale* **2014**, *6*, 3173–3181.

[46] Chen, Z.; Yu, A. P.; Higgins, D.; Li, H.; Wang, H. J.; Chen, Z. W. Highly active and durable core-corona structured bifunctional catalyst for rechargeable metal-air battery application. *Nano Lett.* **2012**, *12*, 1946–1952.

[47] Qian, Y. H.; Hu, Z. G.; Ge, X. M.; Yang, S. L.; Peng, Y. W.; Kang, Z. X.; Liu, Z. L.; Lee, J. Y.; Zhao, D. A metal-free ORR/OER bifunctional electrocatalyst derived from metal-organic frameworks for rechargeable Zn-air batteries. *Carbon* **2017**, *111*, 641–650.